J. Fluid Mech. (1987), *vol.* 184, *pp.* 533–549
Printed in Great Britain

A boundary-element analysis of flagellar propulsion

By N. PHAN-THIEN, T. TRAN-CONG AND M. RAMIA†
Department of Mechanical Engineering, Sydney University, NSW 2006, Australia

(Received 17 July 1986 and in revised form 16 January 1987)

The swimming of a flagellar micro-organism by the propagation of helical waves along its flagellum is analysed by a boundary-element method. The method is not restricted to any particular geometry of the organism nor does it assume a specific wave motion for the flagellum. However, only results for an organism with a spherical or ellipsoidal cell body and a helically beating flagellum are presented here.

With regard to the flagellum, it is concluded that the optimum helical wave (amplitude α and wavenumber k) has $\alpha k \approx 1$ (pitch angle of 45°) and that for the optimum flagellar length $L/A = 10$ (L being the flagellar length, A being the radius of the assumed spherical cell body) the optimum number of wavelengths N_λ is about 1.5. Furthermore there appears to be no optimal value for the flagellar radius a, with the thinner flagella being favoured. These conclusions show excellent quantitative agreement with those of slender-body theory.

For the case of an ellipsoidal cell body, the optimum aspect ratios B/A and C/A of the ellipsoid are about 0.7 and 0.3 respectively; A, B and C are the principal radii of the ellipsoid. These and all of the above conclusions show good qualitative agreement with experimental observations of efficiently swimming micro-organisms.

1. Introduction

This paper is concerned with some hydrodynamic aspects of the swimming of flagellar micro-organisms. There are many groups of micro-organisms possessing flagella, but we are only interested in the single-flagellar varieties such as the spermatozoa of many mammals, many types of protozoa and flagellar bacteria. These micro-organisms, except the flagellar bacteria (they are usually an order-of-magnitude smaller), comprise a somewhat ellipsoidal cell body (head) with a mean radius of ≈ 5 μm and a thin long flagellum (tail) of length ≈ 50 μm and cross-sectional radius of ≈ 0.1 μm. The tail is joined to the head via a mid-piece which may not be present in some micro-organisms. The flagellum of a given organism, in executing some form of wave motion (i.e. helical), induces a propulsive force and an associated torque on the cell body. As a result the whole organism acquires a swimming speed $\boldsymbol{U}$ and a rigid-body counter-rotation $\boldsymbol{\Omega}$. It is the prediction of this swimming speed $\boldsymbol{U}$ and angular velocities $\boldsymbol{\Omega}$ that we are concerned with, given the geometry of the micro-organism and the manner in which waves are passed down the flagellum. This field of study has been appropriately termed flagellar hydrodynamics and has been thoroughly reviewed by Lighthill (1976).

Early mathematical models for flagellar motions were developed by Taylor (1951,

† School of Mechanical and Industrial Engineering, University of New South Wales, P.O. Box 1, Kensington, NSW 2033, Australia.

1952) in which the flagellum was modelled first by a waving infinite sheet and later by a waving cylindrical filament. The former model has the obvious limitation of being based on an assumed two-dimensional flow field. The latter is valid only for wave motions with amplitudes that are small in comparison to the flagellar radius. Most flagellar micro-organisms, however, swim by passing large-amplitude waves down the flagellum. Models for these large-amplitude motions were first proposed by Hancock (1953). His method was to place a distribution of stokeslets and doublets along the centreline of the flagellum. The unknown strengths of these singularities were found by imposing the no-slip boundary conditions approximately at the surface of the flagellum (modelled as a cylindrical filament). However, Hancock's method did not account for the inert head (cell body) which is present in most flagellar micro-organisms. Gray & Hancock (1955) developed a technique (resistive-force theory) that accounted for the cell-body drag. This theory supposes that each point along the flagellum experiences a resistive force which is proportional to the difference between the velocity of the flagellum at that point and the velocity of the surrounding fluid. The coefficient of proportionality is actually a second-order tensor which has two distinct components when expressed in a right-handed orthonormal triad, one of which is locally parallel to the flagellum. One component, K_t, is the resistance coefficient for the relative motion locally tangential to the flagellum; the other, K_n, is the resistance coefficient for the relative motion locally normal to the flagellum. For a slender body K_n is approximately twice K_t. The total propulsive thrust is simply the integral sum of the resistive force acting on the flagellum. This thrust is exactly balanced by the drag force on the cell body which, in turn, yields the swimming velocity of the body. Gray & Hancock (1955) adopted a set of resistance coefficients which were derived from Hancock's previous work with planar waves and applied the resistive-force theory to analyse the motion of a flagellar micro-organism that swims by passing sinusoidal planar waves down its flagellum. The predicted velocity agreed well with observed data on the swimming speed of spermatozoa of sea urchins.

Resistive-force theory can also be extended to cover the helical-wave case. However, Chwang & Wu (1971) noted that the propagation of helical waves along the flagellum induces a torque on the micro-organism. Thus, the body also rotates with an angular velocity in response to this propulsive torque. Based on Gray & Hancock's resistance coefficients, Chwang & Wu (1971) derived expressions for the swimming and angular velocities as well as power requirements. These expressions were then used to determine the optimum proportions of a given micro-organism.

Most bacteria and Eukaryotic micro-organisms swim by passing helical waves along their flagella. This is accomplished by either rotating the filament as a whole, as in the case of bacteria, or by passing bending waves along the flagellum, as in the case of the Eukaryotic micro-organisms (Lighthill 1976). Resistive-force theory can, therefore, be considered as a successful application of hydrodynamics in biology. However, its value as a quantitative tool depends heavily on the accuracy of the resistance coefficients. Lighthill (1976) addressed this important question and rightly pointed out that there were some inconsistencies in Gray & Hancock's resistance coefficients. He derived a set of resistance coefficients that have a better error estimate than is possible with the conventional slender-body theory and applied his theory to the helically beating flagella.

Higdon (1979*a*, *b*, *c*) developed an improved slender-body theory in which the Stokes equations were transformed into a system of singular integral equations in terms of the swimming velocity, angular velocity and force distribution along the

flagellum. These integral equations incorporated an image system inside the spherical cell body whilst allowing for variation in the stokeslet strengths along the flagellar centreline. This accounts for the hydrodynamic interaction between different parts of the flagellum as well as that between the flagellum and the cell body.

Higdon's method represents the state of the art in modelling flagellar hydrodynamics; however it has two major limitations. First, it assumes a spherical cell body, which is rarely the case in reality. Secondly, the inherent error in the slender-body theory is $O(a/L)^2$ (where a and L are the flagellar radius and length respectively), hence significant errors may result for non-'slender' flagellar. There are some micro-organisms in which both these limitations are significant. One example is the Spirillum Volutan, for which no slender-body-theory model presently exists. Chwang, Wu & Winet (1972) presented a resistive-force-theory model for this organism that neglects the flagellar/cell body interaction.

In this paper, we describe a numerical technique for solving flagellar hydrodynamics problems which is based on a boundary-element method and does not assume any specific geometry for the cell body or the flagellum. However we only present results for a micro-organism with a spherical/ellipsoidal cell body and a cylindrical flagellum executing helical wave motion, while a model for the swimming of the Spirillum Volutan will hopefully be presented in a future paper.

2. Analysis

2.1. *Boundary-integral formulation*

The boundary-integral formulation for linear elastic problems (including the Stokes flow problems) is well known and has been well documented elsewhere, e.g. Banerjee & Butterfield (1981) and Brebbia, Telles & Wrobel (1984). The chief advantage of the method is the automatic treatment of flow conditions at infinity; only the boundary of the body, or bodies, requires discretization. Here, we briefly review the method as applied to the Stokes flow problems. We start with the conservation equations

$$\nabla \cdot \boldsymbol{u} = 0, \quad \nabla P = \eta \nabla^2 \boldsymbol{u}, \quad \boldsymbol{x} \in V, \tag{1}$$

where $\boldsymbol{u}$ is the velocity vector, P is the hydrostatic pressure which arises owing to the incompressibility constraint, η is the constant viscosity of the fluid and V is the flow domain. The flow domain is external to the particle (the micro-organism) which has a surface S. On S the no-slip boundary condition applies and we have

$$\boldsymbol{u}(\boldsymbol{x}) = \bar{\boldsymbol{u}}(\boldsymbol{x}), \quad \boldsymbol{x} \in S, \tag{2}$$

where $\bar{\boldsymbol{u}}(\boldsymbol{x})$ is the prescribed velocity of the particle at point $\boldsymbol{x}$. We leave $\bar{\boldsymbol{u}}$ as yet unspecified. Far away from the particle, quiescent conditions apply, i.e. both velocity and traction fields go to zero. Note that there are neither body nor inertial forces in the Stokes equations. These equations are applicable to the motion of fluid around the micro-organism; the Reynolds number based on the lengthscale of the organism is extremely small. The reduction of (1) and (2) to an integral equation is accomplished by using Somigliana's identity

$$u_j(\boldsymbol{X}) = \int_S G_{ij}(\boldsymbol{x}, \boldsymbol{X})\, t_i(\boldsymbol{x})\, \mathrm{d}S(\boldsymbol{x}) - \int_S H_{ij}(\boldsymbol{x}, \boldsymbol{X})\, u_i(\boldsymbol{x})\, \mathrm{d}S(x), \tag{3}$$

where $G_{ij}(\boldsymbol{x}, \boldsymbol{X})$ is the singular stokeslet solution and $H_{ij}(\boldsymbol{x}, \boldsymbol{X})$ is its associated traction field on S:

$$G_{ij}(\boldsymbol{x}, \boldsymbol{X}) = \frac{1}{8\pi\eta r}\left(\delta_{ij} + \frac{r_i r_j}{r^2}\right), \tag{4}$$

$$H_{ij}(\boldsymbol{x}, \boldsymbol{X}) = -\frac{3}{4\pi\eta r^5} r_i r_j \boldsymbol{r}\cdot\boldsymbol{n}, \tag{5}$$

in which $\boldsymbol{r} = \boldsymbol{x} - \boldsymbol{X}$, $r^2 = \boldsymbol{r}\cdot\boldsymbol{r}$, δ_{ij} is the Kronecker delta and $\boldsymbol{n}$ is a unit outward (with respect to the flow domain) normal on S; $\boldsymbol{u}$ and $\boldsymbol{t}$ are respectively the velocity and traction field.

Taking $\boldsymbol{X}$ to a boundary point on S by the usual limiting process yields

$$C_{ji}(\boldsymbol{X})\, u_i(\boldsymbol{X}) + \int_S H_{ij}(\boldsymbol{x}, \boldsymbol{X})\, u_i(\boldsymbol{x})\, \mathrm{d}S(\boldsymbol{x}) = \int_S G_{ij}(\boldsymbol{x}, \boldsymbol{X})\, t_i(\boldsymbol{x})\, \mathrm{d}S(\boldsymbol{x}),$$

$$C_{ij}(\boldsymbol{X}) = \lim_{\epsilon\to 0} \int_{S_\epsilon} H_{ij}(\boldsymbol{x}, \boldsymbol{X})\, \mathrm{d}S(\boldsymbol{x}), \tag{6}$$

where S_ϵ is the surface of V_ϵ, which is the part of the domain contained within a sphere of radius ϵ centred at point $\boldsymbol{X}$. If the surface S is smooth in the sense that it has a tangent plane everywhere, then $C_{ij} = \frac{1}{2}\delta_{ij}$. It should be noted that the integral on the left-hand side of (6) is understood to be a Cauchy principal value integral. A simplification of (6) is possible when the body is undergoing a rigid-body translational motion (Youngren & Acrivos 1975), a rigid-body rotation or both (Tran-Cong & Phan-Thien 1986). The unknown traction on the surface S can be found by solving (6) numerically. In the case of a mixed boundary-value problem, where the velocity is prescribed on part of S, say S_1, and the traction on the remaining part S_2, a rearrangement of (6) is necessary before solving for the unknown traction on S_1 and the unknown velocity on S_2. When a boundary solution has been found (6) can be used again to find the velocity field anywhere in the flow domain (with the convention that $C_{ij}(\boldsymbol{X}) = \delta_{ij}$ when $\boldsymbol{X}$ is inside the open connected domain V).

2.2. *Geometrical modelling*

Although the boundary-integral method is applicable to an arbitrarily shaped body, we choose to analyse the motion of a single flagellar micro-organism that has a spherical or ellipsoidal cell body and swims by executing helical waves down its flagellum. The problem of describing the centreline of the flagellum in this case has been discussed at length by Higdon (1979*c*). Specifically, the position of any point along the centreline of the flagellum is given parametrically by

$$(x, y, z) = (x, \alpha\cos(kx - \omega t), \alpha\sin(kx - \omega t)), \tag{7}$$

where α is the amplitude, k is the wavenumber and ω is the angular frequency of the helical wave.

To place the cell body on the helical axis, Higdon suggested, and we adopt it here, that (7) be slightly modified such that

$$\boldsymbol{r} = (x, y, z) = (x, \alpha E(x)\cos(kx - \omega t), \alpha E(x)\sin(kx - \omega t)), \tag{8}$$

$$E(x) = 1 - \exp(-(k_E x)^2), \tag{9}$$

where k_E is a constant which determines how quickly the helix grows to its maximum amplitude αE. At $x = x_e = 2/k_E$, $E \approx 0.98$ and thus for $x > x_e$ all the wave para-

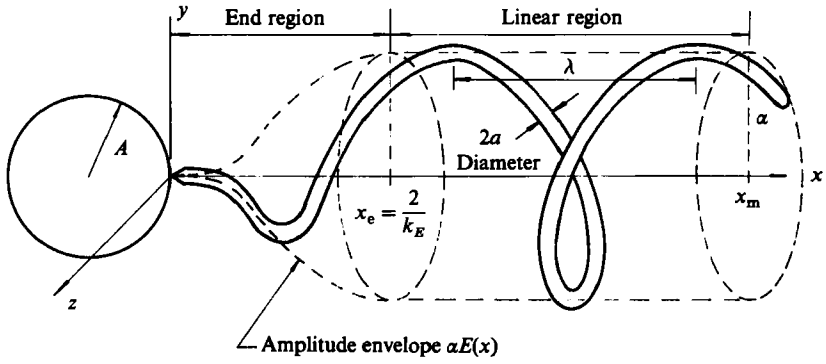

FIGURE 1. The micro-organism as modelled by a spherical cell body attached to the helically beating flagellum.

meters are essentially constant. This region is called the linear region. In the region $0 < x \leqslant x_e$ all the wave parameters are functions of x; it is called the end region, refer to figure 1. A realistic proportion for these regions is $x_e/x_m \approx \frac{1}{3}$, where x_m is the maximum x-coordinate of the flagellum; a realistic choice for k_E can then be made accordingly ($k_E \approx 1$). We now assume that the flagellum is simply a cylindrical filament of cross-sectional radius a. It can be shown (by using the symbolic manipulation system Macsyma) that any point P on the surface of this filament has the coordinates

$$(x+H(x,\phi), \alpha E\cos\theta+M(x,\phi), \alpha E\sin\theta+N(\alpha,\phi)), \tag{10}$$

where $\theta = kx-\omega t$ and $0 \leqslant \phi < 2\pi$ is the polar angle on a plane orthogonal to the centreline of the flagellum and passing through P. H, M and N are some functions of x and ϕ; they are given in Appendix A. The total length of the flagellum is given by

$$L = \int_0^{\lambda N_\lambda} \left[1+\left(\frac{\partial r_y}{\partial x}\right)^2+\left(\frac{\partial r_z}{\partial x}\right)^2\right]^{\frac{1}{2}} \mathrm{d}x, \tag{11}$$

where r_y, r_z are given in (8), $\lambda = 2\pi/k$ is the wavelength of the flagellum and N_λ is the number of wavelengths. It is generally agreed that the flagellum is inextensible and hence L must remain constant. We thus allow the wave parameters $(\alpha k, N_\lambda, k/k_E)$ to vary at will, calculate the length L from (11) and from the given values $a/A, L/A$ calculate the body parameters a and A; A is some characteristic radius of the cell body.

Using (10) we model the cylindrical filament as a series of either hexagonal (or pentagonal) cylinders; the surface of each cylinder is further divided into triangular elements. The free end of the flagellum, $x = x_m$, is used as the apex of an hexagonal (or pentagonal) pyramid representing the end segment.

In an attempt to quantify the variation in discretization error with the number of boundary elements on the cell body, three different discretization schemes were employed. Coxeter (1975) gives the coordinates of the vertices of an icosahedron. By lifting the midpoint of each edge out to the surface of the sphere and using the extra 30 resulting vertices, the sphere can be descretized into 80 elements. The coordinates of the vertices of an octahedron are as given in Appendix B. Again by lifting the midpoint of each edge to the surface, the sphere can be discretized into 32 elements.

The elipsoidal cell body was discretized by scaling the vertices of the corresponding

Ratio of semi-major to semi-minor axes (A/C)	Error in drag prediction on a spheroid in axial flow (%)		
	20 elements	32 elements	80 elements
0.1	5.15	1.07	1.44
0.2	4.77	1.38	1.23
0.5	4.69	2.44	1.35
0.6	4.69	2.79	0.419
0.7	6.66	2.54	1.18
0.8	0.250	3.23	1.28
0.9	5.63	3.17	1.41
1	4.17	3.25	1.33
1.1	4.54	3.32	1.36
1.5	4.35	3.46	1.38
2	4.54	3.42	1.34
5	4.48	2.78	1.35
10	4.39	2.53	1.33
20	4.18	2.19	1.30
Mean percentage error	4.46	2.68	1.26

TABLE 1

Ratio of semi-major to semi-minor axes (A/C)	Error in drag prediction on a spheroid in transverse flow (%)		
	20 elements	32 elements	80 elements
0.1	4.02	1.91	1.18
0.2	4.08	2.46	1.25
0.5	4.45	3.22	1.46
0.6	4.41	3.27	1.23
0.7	4.93	3.35	1.27
0.8	2.79	3.35	1.24
0.9	4.89	3.33	1.28
1	4.17	3.25	1.33
1.1	4.35	3.21	1.37
1.5	4.68	3.02	1.30
2	4.43	2.78	1.33
5	3.98	1.97	1.24
10	3.48	1.35	1.13
20	2.80	0.228	0.903
Mean percentage error	4.10	2.62	1.25

TABLE 2

discretized sphere according to the aspect ratios of the ellipsoid. Hence a vertex (x, y, z) lying on a sphere of radius A is mapped onto a vertex $(x, (B/A)y, (C/A)z)$ lying on an ellipsoid of principal radii A, B and C. Finally, a correction factor is applied to the radii of the spherical/ellipsoidal cell bodies so that the actual surface areas of the cell bodies and those of the corresponding discretized cell bodies are identical.

Each of the above discretization schemes was used to predict the drag on a spheroid (both for axial and transverse flow) and the results compared with the exact solution of Happel & Brenner (1973). The resulting errors are as summarized in tables 1 and 2. It is apparent that the error is quite insensitive to the aspect ratio of the spheroid

and type of flow. Furthermore, for the 80-element cell body, the average error is about 1.3%.

If the angular frequency of the helical waves is ω, cf. (8), then the centreline of the flagellum appears to rotate relative to the cell body with the same angular velocity ω. We shall assume that the cylindrical flagellum also rotates rigidly relative to the cell body with an angular velocity of ω. A different mode of rotation can also be accommodated, but is not considered here. The kinematic constraint then requires that the flagellum be joined to the cell body at one single point. This is done by using an hexagonal (or pentagonal) pyramid to represent the first segment in the end region of the flagellum. Figures 2–8 illustrate some final boundary-discretization meshes.

2.3. *Numerical procedure*

We use constant boundary elements and assume that both the velocity and the traction fields remain constant within a triangular element. Equation (6) is reduced to

$$C_{ji}u_i^{(k)} + \sum_{n=1}^{N} u_i^{(n)} \int_{S_n} H_{ij}(\boldsymbol{x}, \boldsymbol{X})\, \mathrm{d}S(\boldsymbol{x}) = \sum_{n=1}^{N} t_i^{(n)} \int_{S_n} G_{ij}(\boldsymbol{x}, \boldsymbol{X})\, \mathrm{d}S(\boldsymbol{x}), \tag{12}$$

where $\boldsymbol{u}^{(n)}$ and $\boldsymbol{t}^{(n)}$ are the velocity and the traction on element n. Point $\boldsymbol{X}$ belongs to element k and $\boldsymbol{x}$, to element n. Some integrals in (12) can be calculated analytically (Brebbia *et al.* 1984), those remaining are evaluated numerically using a 64-point Gaussian quadrature scheme. Equation (12) is then arranged in the form

$$\boldsymbol{Hu} = \boldsymbol{Gt}, \tag{13}$$

where $\boldsymbol{H}, \boldsymbol{G}$ are known $[3N, 3N]$ matrices and $\boldsymbol{u}$ and $\boldsymbol{t}$ are the boundary-solution velocity and traction vectors (of dimension $3N$). They are arranged such that u_1, u_2, u_3 are the components of the velocity vector $\bar{\boldsymbol{u}}$ at element 1, etc. Note that both $\boldsymbol{H}$ and $\boldsymbol{G}$ depend only on the geometry of the body, not on the prescribed boundary conditions.

Now on the surface of the body the velocity field takes the form

$$\bar{\boldsymbol{u}}(x) = \begin{cases} \boldsymbol{U} + \boldsymbol{\Omega} \times \boldsymbol{x}, & \text{if } \boldsymbol{x} \text{ is on the cell body,} \\ \boldsymbol{U} + (\boldsymbol{\Omega} - \boldsymbol{\omega}) \times \boldsymbol{x}, & \text{if } \boldsymbol{x} \text{ is on the flagellum,} \end{cases} \tag{14}$$

where $\boldsymbol{U}$ is the instantaneous swimming velocity of the body and $\boldsymbol{\Omega}$ is the rigid body angular velocity of the cell body. The flagellum rotates with respect to the rest frame with an angular velocity of $(\boldsymbol{\Omega} - \boldsymbol{\omega})$. Both $\boldsymbol{U}$ and $\boldsymbol{\Omega}$ (a total of six components) are yet unknown. However, the micro-organism is self-propelled and not influenced by any external forces. Therefore, the total force and moment on the micro-organism are zero. Thus,

$$\sum_{n=1}^{N} S_n \boldsymbol{t}^{(n)} = 0; \quad \sum_{n=1}^{N} S_n \boldsymbol{x}^{(n)} \times \boldsymbol{t}^{(n)} = 0, \tag{15}$$

where S_n is the area of the element n, $\boldsymbol{t}^{(n)}$ is the traction vector on this element and $\boldsymbol{x}^{(n)}$ is the position of the centroid of this element. From (13) one has symbolically,

$$\boldsymbol{t} = \boldsymbol{G}^{-1}\boldsymbol{Hu} \tag{16}$$

noting that both $\boldsymbol{G}$ and $\boldsymbol{H}$ are known for any given surface geometry; $\boldsymbol{G}^{-1}$ is the inverse of $\boldsymbol{G}$. It can now be clearly seen that once (16) is substituted in (15) with the help of (14), a system of six equations results from which $\boldsymbol{U}$ and $\boldsymbol{\Omega}$ can be solved for.

Once the unknown velocities $\boldsymbol{U}$ and $\boldsymbol{\Omega}$ are found, the unknown traction vector can be recovered from (16) and thus the flow field around the body is fully determined,

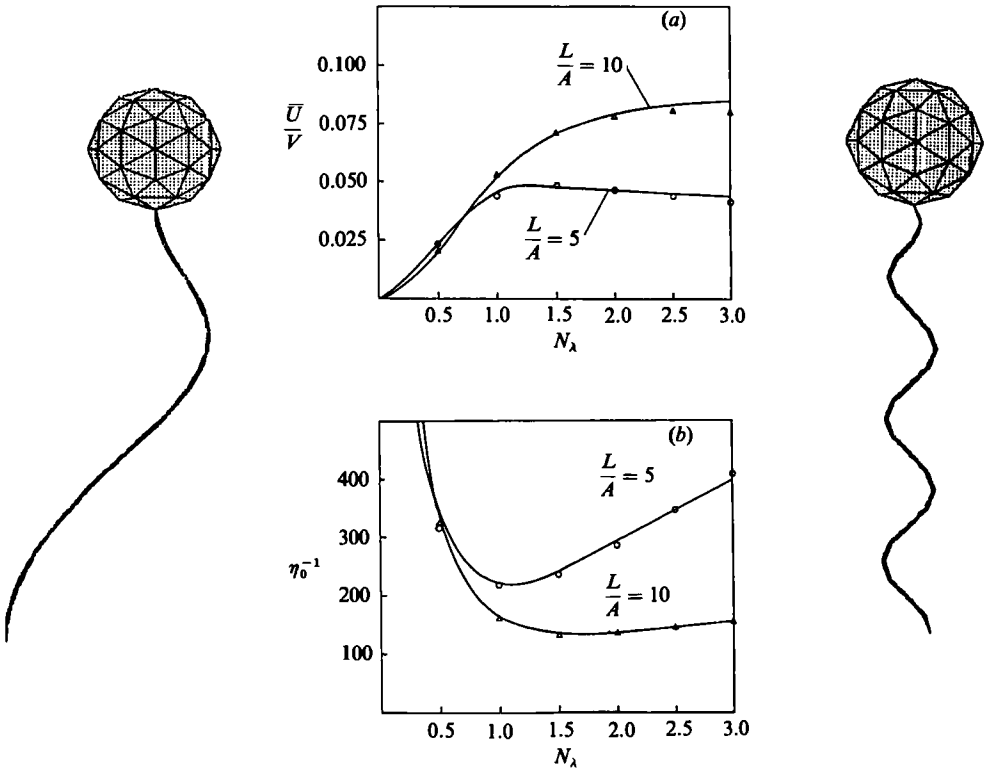

FIGURE 2. (*a*) Non-dimensional mean swimming speed and (*b*) inverse efficiency as functions of the wave parameter N_λ (for a spherical cell body, $\alpha k = 1$, $k/k_E = 1$ and $a/A = 0.02$): ○, boundary-element results for $L/A = 5$; △, boundary-element results for $L/A = 10$; ——, slender-body-theory results of Higdon. On the left is the boundary element mesh for an organism with the above-mentioned parameter values ($L/A = 10$) and $N_\lambda = 0.5$; on the right is that for an organism with $N_\lambda = 3$.

cf. (6). The program was written in FORTRAN for the VAX/780 and a 32-bit microcomputer (DSI co-processor board hosted by an IBM-PC). Implementation on smaller personal computers such as Apricot can and has been done; however, the solution procedure is based on a block-partition method (see, for example, Tran-Cong & Phan-Thien 1986). It should be noted that the conditioning number of the system matrix is quite large (of the order 300). Double-precision arithmetic needs to be used to invert the matrix $\boldsymbol{G}$. Here we adopt the standard Gauss–Jordan elimination method in double-precision mode.

3. Results

Keller & Rubinow (1976) showed that the swimming trajectory for a micro-organism with a helically beating flagellum is itself helical. They derived analytical expressions for the radius, period and pitch angle of the trajectory in terms of the instantaneous swimming velocity and angular velocity. Furthermore, the velocity of the organism along the axis of the helical trajectory $\overline{U}$ is constant and is given by

$$\overline{U} = \overline{\boldsymbol{U}} \cdot \frac{(\boldsymbol{\Omega} - \omega)}{|\boldsymbol{\Omega} - \omega|}. \tag{17}$$

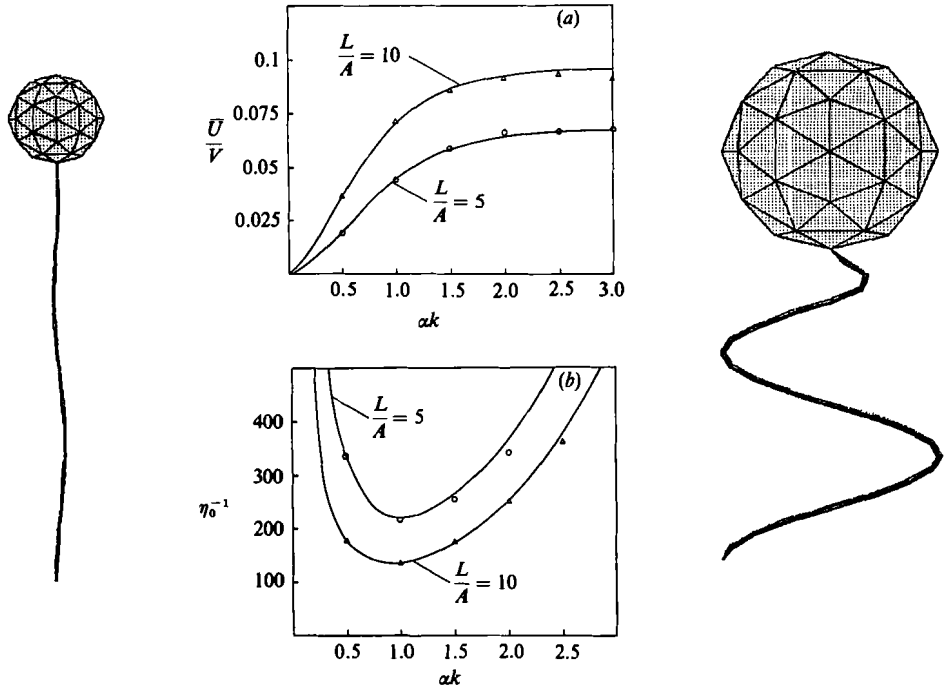

FIGURE 3. (*a*) Non-dimensional mean swimming speed and (*b*) inverse efficiency as functions of the wave parameter αk (for a spherical cell body, $N_\lambda = 1$ for $L/A = 5$, $N_\lambda = 1.5$ for $L/A = 10$, $k/k_E = 1$ and $a/A = 0.02$): ○, boundary-element results for $L/A = 5$; △, boundary-element results for $L/A = 10$; ——, slender-body-theory results of Higdon. On the left is the boundary element mesh for an organism with the above-mentioned parameter values ($L/A = 10$) and $\alpha k = 0.1$; on the right is that for an organism with $\alpha k = 3$.

Hence $\overline{U}$ can be calculated by solving the problem at one instant of time. This argument however assumes an axisymmetric cell body, hence it generally does not apply to the case of an ellipsoidal cell body. In this case, one needs to solve the problem for several different configurations of the flagellum (relative to the cell body) and determine the mean of the calculated velocities. This is then normalized with respect to the linear speed of the flagellar wave ($V = \omega/k$).

Of primary interest here is the mean power dissipation, $\overline{P}$, in swimming. Again, for an axisymmetric cell body, this is equal to the instantaneous power dissipation P and is given by

$$\overline{P} = -\sum_{n=1}^{N} S_n \boldsymbol{t}^{(n)} \cdot \boldsymbol{u}^{(n)}.$$

This power consumption can be easily shown to be $-\boldsymbol{T}\cdot\boldsymbol{w}$, where $\boldsymbol{T}$ is the torque acting on the flagellum. This is non-dimensionalized with respect to $6\pi\eta\overline{A}\,\overline{U}^2$ (where $\overline{A}$ is the volume average radius of the cell body) to give the inverse efficiency

$$\eta_0^{-1} = \frac{\overline{P}}{6\pi\eta\overline{A}\,\overline{U}^2},$$

as its minimum defines the optimal swimming motion for the micro-organism.

In the case of an ellipsoidal cell body, neither $(\overline{U}/V)$ nor η_0^{-1} vary by more than

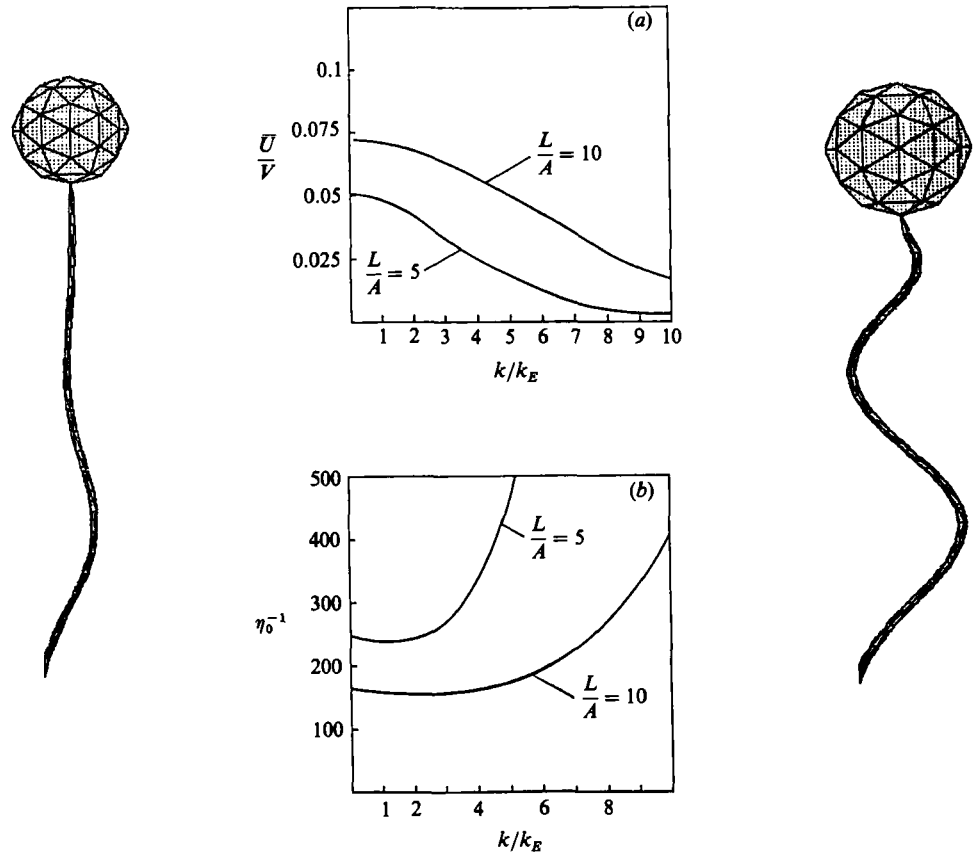

FIGURE 4. (*a*) Non-dimensional mean swimming speed and (*b*) inverse efficiency as functions of the wave parameter k/k_E (for a spherical cell body, $\alpha k = 1$, $N_\lambda = 1$ for $L/A = 5$, $N_\lambda = 1.5$ for $L/A = 10$, $a/A = 0.05$): ——, boundary-element results. On the left is the boundary element mesh for an organism with the above-mentioned parameter values ($L/A = 10$) and $k/k_E = 10$; on the right is that for an organism with $k/k_E = 1$.

2% throughout a given flagellar cycle. Hence it seems that investigation of eight different instants in a given cycle is sufficient.

The mean swimming speed and inverse efficiency are functions of seven parameters: the wave parameters N_λ, αk and k/k_E and the body parameters $a/\bar{A}$, $L/\bar{A}$, B/A and C/A. First, assuming a spherical cell body, the optimum wave parameters (for typical body parameters) are determined. Then fixing the wave parameters at their optimum values (and still assuming a spherical cell body) the parameters $a/\bar{A}$ and $L/\bar{A}$ are optimized. The next step is to fix all other parameters at their optimal values and assume the cell body to be a spheroid, hence the optimal aspect ratio B/A is determined. Finally C/A is optimized by allowing the cell body to be an asymmetric ellipsoid.

All the results shown in figures 2–8 can be explained in terms of the following three qualitative concepts of flagellar hydrodynamics (Higdon 1979*c*):

(i) The role of the resistance coefficients: The propulsive effect of the flagellum is due to the resistance to normal motion being much larger than that to tangential

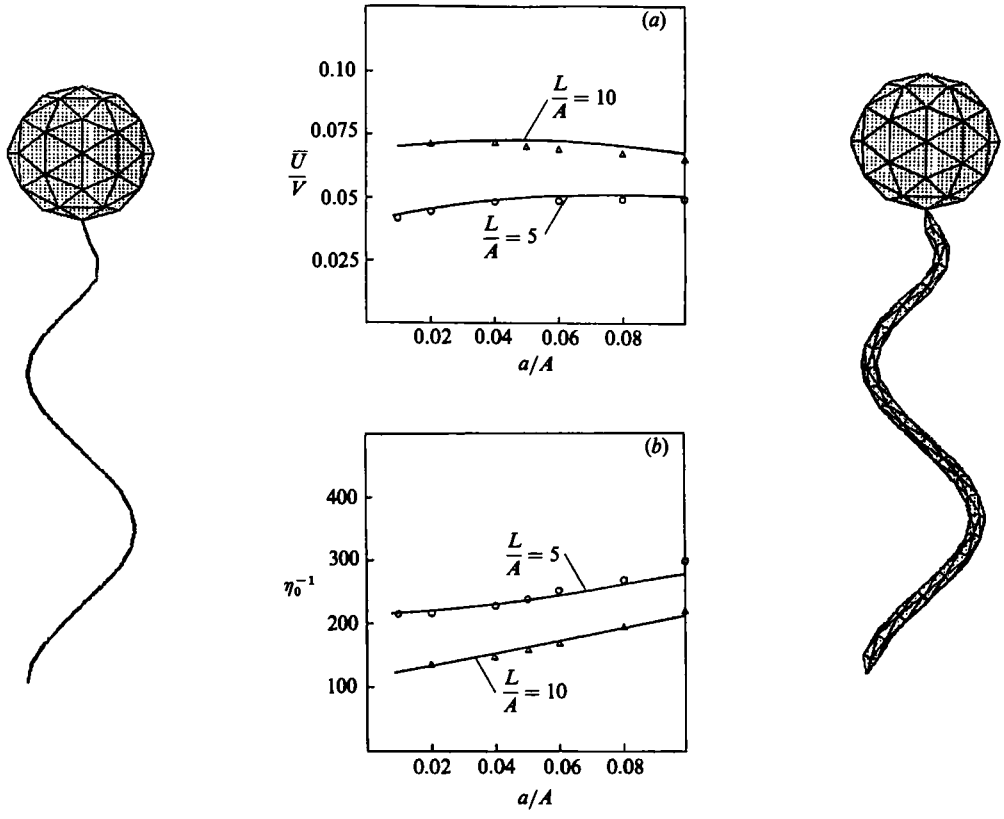

FIGURE 5. (*a*) Non-dimensional mean swimming speed and (*b*) inverse efficiency as functions of the body parameter a/A (for a spherical cell body, $\alpha k = 1$, $k/k_E = 1$, $N_\lambda = 1$ for $L/A = 5$, $N_\lambda = 1.5$ for $L/A = 10$): ○, boundary-element results for $L/A = 5$; △, boundary-element results for $L/A = 10$; ——, slender-body-theory results of Higdon. On the left is the boundary-element mesh for an organism with the above-mentioned parameter values ($L/A = 10$) and $a/A = 0.01$; on the right is that for an organism with $a/A = 0.1$.

motion. The important parameter in these coefficients is the slenderness ratio λ/a (Lighthill 1976). Increasing this slenderness ratio has the effect of increasing K_n relative to K_t, hence the mechanism is more effective, leading to an increase in swimming speed. Furthermore η_0^{-1} decreases with each of the resistance coefficients and with increasing swimming speed. In summary, it can be assumed that an increase in the slenderness ratio improves the efficiency of the organism in question as it leads to an increased swimming speed together with an independent decrease in the power consumed.

(ii) The role of the counter-rotation with angular velocity Ω (assumed to be primarily along the axis of the helix). The swimming speed is proportional to the effective rotation rate of the flagellum $\omega - \Omega$. Ω is less than or equal to ω and increases with the torque T (which the flagellum induces on the cell body) which in turn is proportional to $a\alpha^2 L$. Similarly, the force that the flagellum induces on the cell body F is proportional to $a\alpha L$ and the swimming speed increases with this propulsive force. Furthermore η_0^{-1} increases with T because rotation of the cell body is very power consuming and decreases with F via an increase in $\bar{U}$.

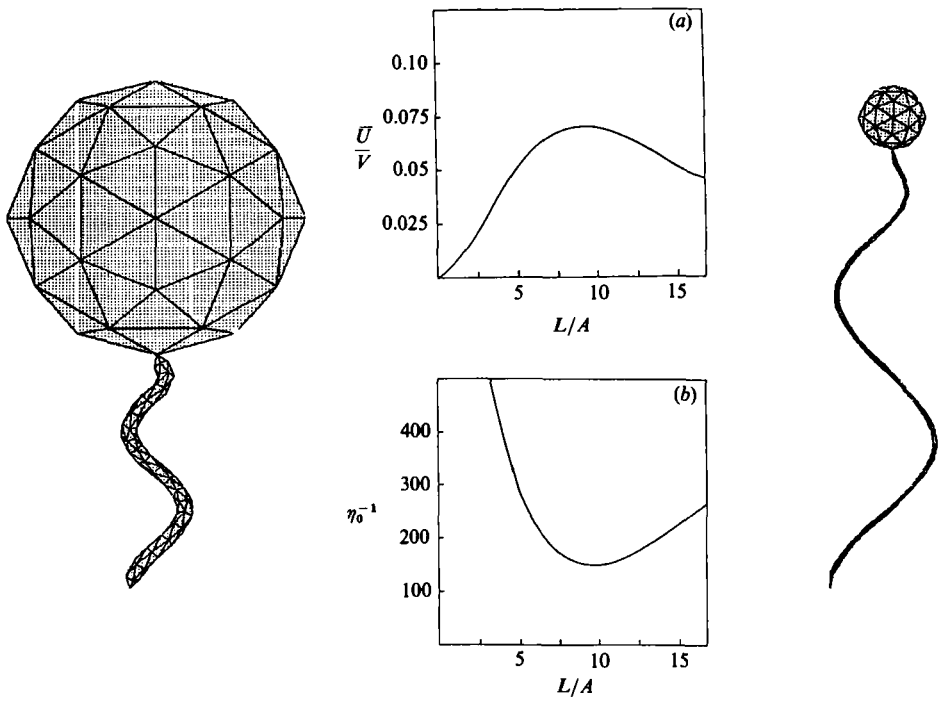

FIGURE 6. (*a*) Non-dimensional mean swimming speed and (*b*) inverse efficiency as functions of the body parameter L/A (for a spherical cell body, $\alpha k = 1$, $k/k_E = 1$, $N_\lambda = 1.5$ and $a/A = 0.05$): ——, boundary-element results. On the left is the boundary element mesh for an organism with the above-mentioned parameter values and $L/A = 2.5$; on the right is that for an organism with $L/A = 20$.

(iii) The effect of hydrodynamic interaction between neighbouring waveforms of the flagellum and/or between the flagellum and the cell body. This is a purely detrimental effect as it leads to a decrease in the swimming speed with an independent increase in the inverse efficiency.

Figure 2 shows the swimming speed and inverse efficiency as functions of the wave parameter N_λ (with $\alpha k = 1, k/k_E = 1, a/A = 0.02$, spherical cell body of radius A). The first thing to note is the excellent agreement between the present results (shown as either △ or ○) and those of Higdon (1979*c*) (shown as solid line): one could mistake the solid line for the line of best fit of the points shown. As the number of wavelengths increases while the waves remain geometrically similar, the amplitude α and wavelength λ of the waves decrease. Initially, for lower values of N_λ, the decrease in α reduces T more severely than it reduces F: hence $(\overline{U}/V)$ increases and η_0^{-1} decreases, see (ii) above. For higher values of N_λ, this effect is offset and eventually overshadowed by the decrease in the slenderness ratio λ/a, (i), and the interaction between neighbouring waveforms of the flagellum, (iii). The optimum values, $N_\lambda = 1$ for $L/A = 5$ and $N_\lambda = 1.5$ for $L/A = 10$, represent the respective points at which the compromise between the above-mentioned effects is at its best.

Figure 3 shows the swimming speed and inverse efficiency as functions of the wave parameter αk ($N_\lambda = 1$ for $L/A = 5$, $N_\lambda = 1.5$ for $L/A = 10$, $k/k_E = 1$, $a/A = 0.02$, spherical cell body). Again, the agreement with slender-body theory is excellent. Increasing the parameter αk has the effect of increasing the amplitude α and

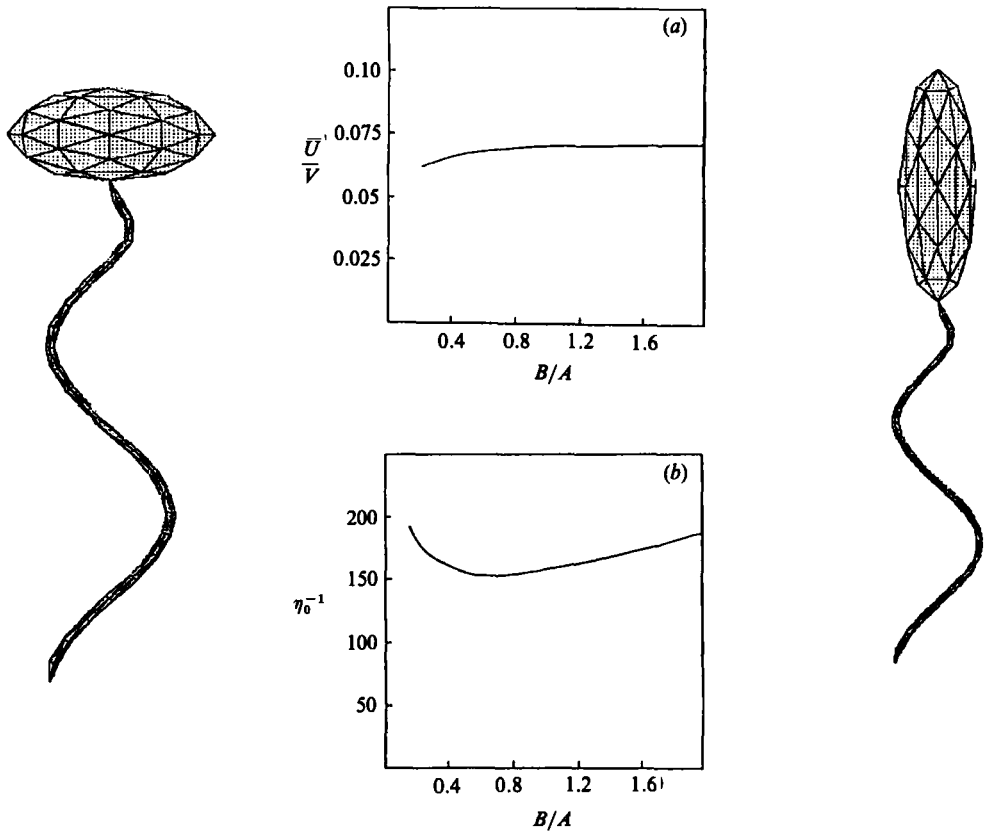

FIGURE 7. (*a*) Non-dimensional mean swimming speed and (*b*) inverse efficiency as functions of the body parameter B/A (where A and B are the principal radii of the spheroidal cell body, A lying along the symmetry axis, $\alpha k = 1$, $k/k_E = 1$, $N_\lambda = 1.5$, $a/A = 0.05$, $L/A = 10$. Here A is the radius of the sphere whose volume is equal to that of the spheroidal cell body): ——, boundary-element results. On the left is the boundary element mesh for an organism with the above-mentioned parameter values and $B/A = 2$; on the right is that for an organism with $B/A = 0.3$.

decreasing the wavelength λ of the flagellar waves. Initially α is so small as to lead to a small propulsive force F, which may be too small to effectively overcome the drag on the cell body. Indeed in the extreme case when $\alpha k = 0$ and the flagellum is axisymmetric, the propulsive force is zero. For larger amplitudes, the increase in the propulsive torque T becomes the more important consideration bringing the increase in $(\overline{U}/V)$ to a halt, (ii). This together with the decrease in the slenderness ratio, (i), eventually negates the effect of the increased propulsive force. Here the compromise is reached at the optimum value $\alpha k = 1$ (pitch angle of 45°) which appears to be independent of the flagellar length.

Figure 4 shows the swimming speed and inverse efficiency as functions of the wave parameter k/k_E ($\alpha k = 1$, $N_\lambda = 1$ for $L/A = 5$, $N_\lambda = 1.5$ for $L/A = 10$, $a/A = 0.005$, spherical cell body). This parameter determines the length of the end region, i.e. how quickly the flagellum grows to its maximum amplitude. It is apparent that the swimming speed decreases consistently with k/k_E while, within a realistic range (depending on the flagellar length) of this parameter, the inverse efficiency is essentially constant. Hence we conclude that the efficiency of the swimming motion

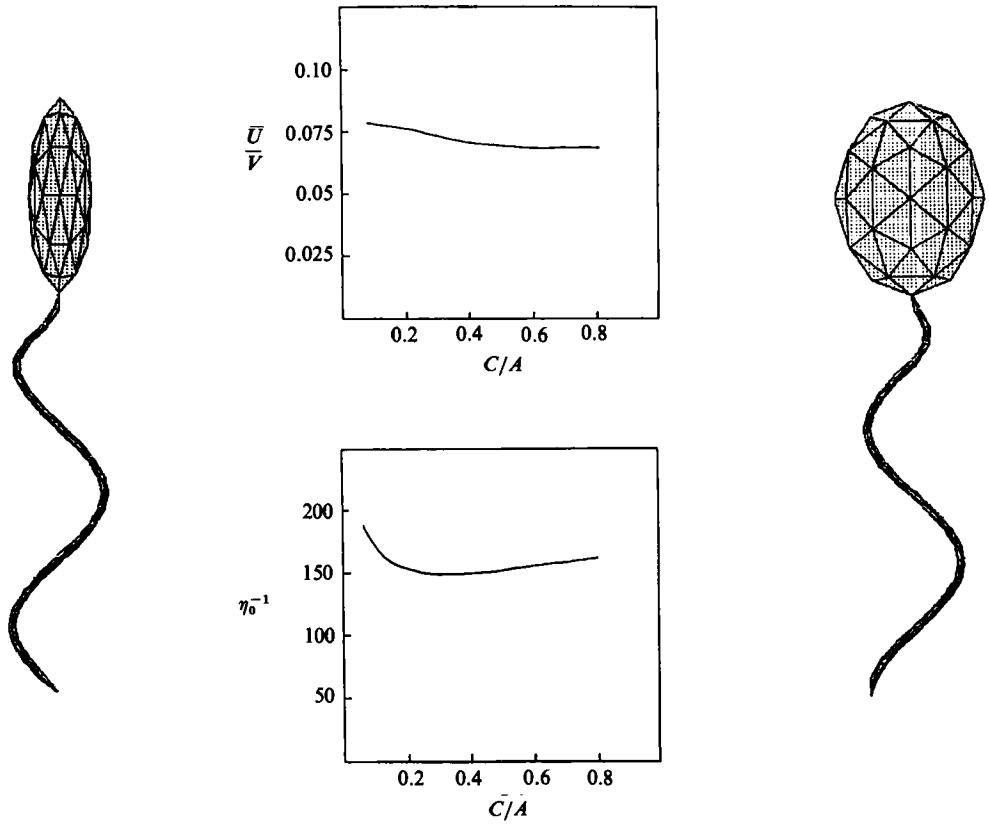

FIGURE 8. (*a*) Non-dimensional mean swimming speed and (*b*) inverse efficiency as functions of the body parameter C/A (where A, B and C are the principal radii of the ellipsoidal cell body with A lying along the axis of the helical flagellum, $\alpha k = 1$, $k/k_E = 1$, $N_\lambda = 1.5$, $a/A = 0.05$, $L/\bar{A} = 10$, $B/A = 0.7$. Again, here, A is the equivalent cell body radius, based on volume conservation): ——, boundary-element results. On the left is the boundary element mesh for an organism with the above-mentioned parameter values and $C/A = 0.3$ (this is the optimal micro-organism); on the right is that for an organism with $C/A = 0.7$.

is fairly insensitive to the parameter k/k_E, provided that the end region does not occupy too large a proportion of the flagellar length.

Figure 5 shows the swimming speed and inverse efficiency as functions of the body parameter a/A ($\alpha k = 1$, $N_\lambda = 1$ for $L/A = 5$, $N_\lambda = 1.5$ for $L/A = 10$, $k/k_E = 1$, spherical cell body). Again agreement with the slender-body theory is excellent. It is apparent that the swimming speed is fairly insensitive to variations in a/A. This is due to the increase in the propulsive force F being offset by the associated increase in the propulsive torque, (ii). The inverse efficiency increases monotonically with a/A, owing to the increasing propulsive torque, (ii), and the decrease in the slenderness ratio, (i). Whilst the thinner flagella are favoured, there appears to be no optimal value for this parameter.

Figure 6 shows the swimming speed and inverse efficiency as functions of the body parameter L/A ($\alpha k = 1$, $N_\lambda = 1.5$, $k/k_E = 1.5$, $a/A = 0.05$, spherical cell body). Initially, the swimming speed increases with an increase in L/A. This is because, for the shorter flagella, the propulsive force F is too small to effectively propel the large cell body, (ii). This together with the diminishing effect of hydrodynamic interaction,

(iii), (which is proportionately more important for shorter flagella) leads to an increase in the swimming speed and a decrease in the inverse efficiency. For larger values of L/A, the effect of the increasing propulsive torque, (ii), overshadows the above-mentioned effects. The point at which these mechanisms reach the best compromise is $L/A = 10$. Direct comparison with Higdon's results cannot be made here as N_λ was kept at its optimum value in the latter (this optimum value depends on L/A).

Figure 7 shows the swimming speed and inverse efficiency as functions of the body parameter B/A ($\alpha k = 1$, $N_\lambda = 1.5$, $L/\overline{A} = 10$, $a/\overline{A} = 0.05$, $C/A = B/A$, $\overline{A}$ is the volume mean radius of the spheroidal cell body). The most important consideration here is that for a given volume, the cell body should have minimum resistance (to axisymmetric translation) while its moment of rotational inertia should be maximized (ii). Bourot (1974) showed that satisfying the former of these constraints leads to a body shape which is nearly a prolate spheroid of aspect ratio about 0.5. This is not too different to the optimal aspect ratio of about 0.7 obtained here.

Figure 8 shows the swimming speed and inverse efficiency as functions of the body parameter C/A ($\alpha k = 1$, $N_\lambda = 1.5$, $k/k_E = 1$, $a/\overline{A} = 0.05$, $L/\overline{A} = 10$, $B/A = 0.7$). Here it is found that for a cell body with minimum translational resistance and maximum rotational resistance, the body parameter C/A is about 0.3. Hence, the optimum cell body shape is a flat elipsoid (of aspect ratios about 0.7 and 0.3). There are many examples of this in nature, see for example Rikmenspoel (1966) who gives the dimensions of a bull spermotozoa.

4. Conclusion

In summary we conclude that the boundary-element method can be successfully applied to solve flagellar hydrodynamics problems. The major contributing factor that renders this feasible is that the traction boundary solution is not very sensitive to the aspect ratios of the triangular boundary elements. This allows the slenderness and curvature associated with flagella to be easily modelled. Meaningful results were obtained for boundary-element meshes in which the majority of the triangular elements have an aspect ratio of about 20. Although the matter was not investigated beyond this point, there may not be as much flexibility for 'non-rigid body' boundary conditions.

The problem of designing an efficiently swimming micro-organism was addressed here. Given that a certain volume of biological material is to be transported as efficiently as possible by a helically beating flagellum, the following conclusions, regarding the proportions and configuration of the organism, were reached:

The optimum shape for the cell body is a flat ellipsoid with aspect ratios of about 0.7 and 0.3; the flagellum should have a length about ten times the volume average radius of the cell body and as small as possible a radius; this flagellum should execute helical wave motion of amplitude α and wavenumber k such that $\alpha k \approx 1$ and curl itself into about 1.5 wavelengths.

The above conclusions show good agreement with experimental observation of efficiently swimming micro-organisms (Rikmenspoel 1966; Leifson 1960). Hence it would appear that the theory regarding the survival of the fittest applies even at this microscopic scale.

This research is supported by the Australian Research Grant Scheme (ARGS). We thank Mr David Tullock for his help with the graphics. We wish to thank the two referees who made numerous suggestions to improve the paper.

Appendix A. Discretization of the flagellum

Assuming that the position vector of a point along the centreline of the flagellum is given by (8) and (9), and that the flagellum is a cylindrical body of radius a, then it can be shown that any point on the surface of the flagellum that lies on the plane orthogonal to the centreline at (x, y, z) has coordinates given by (10) where $0 \leqslant \phi < 2\pi$ is a polar angle and

$$H(x,\phi) = \alpha a \frac{D}{G} \sin\phi, \tag{A 1}$$

$$M(x,\phi) = \frac{a}{G}\left\{\frac{Ek\sin\theta - E'\cos\theta}{D}\sin\phi + (E'\sin\theta + Ek\cos\theta)\cos\phi\right\}, \tag{A 2}$$

$$N(x,\phi) = \frac{a}{G}\left\{(Ek\sin\theta - E'\cos\theta)\cos\phi - \frac{E'\sin\theta + Ek\cos\theta}{D}\sin\phi\right\}, \tag{A 3}$$

$$D = \{1 + \alpha^2(E^2k^2 + E'^2)\}^{\frac{1}{2}}, \tag{A 4}$$

$$G = \{E^2k^2 + E'^2\}^{\frac{1}{2}}, \tag{A 5}$$

where $\theta = kx - \omega t$, E is given by (9) and E' is the derivative of E with respect to x. These expressions were found using a symbolic manipulation system MACSYMA.

Appendix B. Discretization of the spherical cell body

The spherical cell body is discretized into a 20-element, 80-element or a 32-element body. Coxeter (1975) gives the coordinates of the vertices of the 20-element icosahedron as

$$(0, \pm\tau, \pm 1), \quad (\pm 1, 0, \pm\tau), \quad (\pm\tau, \pm 1, 0), \tag{B 1}$$

where τ is an irrational number whose integer powers are given by

$$2\tau^{\pm n} = \begin{cases} f_n\sqrt{5} \pm (f_{n-1} + f_{n+1}), & n \text{ odd}, \\ (f_{n-1} + f_{n+1}) \pm f_n\sqrt{5}, & n \text{ even}, \end{cases}$$

where $\{f_n\} = \{1, 1, 2, 3, 5, 8, 13, \ldots\}$ is the Fibonacci sequence. Coxeter (1974) also gives the coordinates of the vertices of an icosadodecahedron as

$$\left.\begin{gathered} (\pm 2, 0, 0), \quad (0, \pm 2, 0), \quad (0, 0, \pm 2), \\ (\pm\tau, \pm\tau^{-1}, \pm 1), \quad (\pm 1, \pm\tau, \pm\tau^{-1}), \quad (\pm\tau^{-1}, \pm 1, \pm\tau). \end{gathered}\right\} \tag{B 2}$$

By multiplying (B 1) by $A(1+\tau^2)^{\frac{1}{2}}$ and (B 2) by $\frac{1}{2}A$ (for scaling reasons) we can generate all 42 vertices of the 80-element sphere.

To generate the 32-element sphere, one begins with the octahedron (with vertices (B 3a)), and divides each of its triangular faces into four triangles. The coordinates of the resulting vertices are

$$(\pm A, 0, 0), \quad (0, \pm A, 0), \quad (0, 0, \pm A), \tag{B 3a}$$

$$(0, \pm\tfrac{1}{2}A, \pm\tfrac{1}{2}A), \quad (\pm\tfrac{1}{2}A, 0, \pm\tfrac{1}{2}A), \quad (\pm\tfrac{1}{2}A, \pm\tfrac{1}{2}A, 0). \tag{B 3b}$$

REFERENCES

BANERJEE, P. K. & BUTTERFIELD, R. 1981 *Boundary Element Methods in Engineering Science*, McGraw-Hill.

BOUROT, J. M. 1974 On the computation of the optimum profile in Stokes flow. *J. Fluid Mech.* **65**, 513–515.

BREBBIA, C. A., TELLES, C. F. & WROBEL, L. C. 1984 *Boundary Element Techniques: Theory and Application in Engineering*. Springer.

CHWANG, A. T. & WU, T. Y. 1971 A note on helical movement of micro-organisms. *Proc. R. Soc. Lond.* B **178**, 327–346.

CHWANG, A. T., WU, T. Y. & WINET, H. 1972 Locomotion of Spirilla. *Biophys. J.* **12**, 1549–1561.

COXETER, H. 1975 *Regular Complex Polytopes*. Cambridge University Press.

GRAY, J. & HANCOCK, G. J. 1955 The propulsion of sea-urchin spermatozoa. *J. Exp. Biol.* **32**, 802–814.

HANCOCK, G. J. 1953 The self propulsion of microscopic organisms through liquid. *Proc. R. Soc. Lond.* A **217**, 96–121.

HAPPEL, J. & BRENNER, H. 1973 *Low Reynolds Number Hydrodynamics*. Noordhoff.

HIGDON, J. J. L. 1979*a* A hydrodynamics analysis of flagellar propulsion. *J. Fluid Mech.* **90**, 685–711.

HIGDON, J. J. L. 1979*b* The generation of feeding currents by flagellar motion. *J. Fluid Mech.* **94**, 305–330.

HIGDON, J. J. L. 1979*c* The hydrodynamics of flagellar propulsion: helical waves. *J. Fluid Mech.* **94**, 331–351.

KELLER, J. B. & RUBINOW, S. I. 1976 Swimming of flagellated micro-organisms. *Biophys. J.* **16**, 151–170.

LEIFSON, E. 1960 *Atlas of Bacterial Flagellation*. Academic.

LIGHTHILL, M. J. 1976 Flagellar hydrodynamics. The John von Neumann Lecture 1975. *SIAM Rev.* **18**, 161–229.

RIKMENSPOEL, R. 1966 In *Dynamics of Fluids and Plasmas* (ed. T. L. Lincoln), pp. 9–34. Academic.

TAYLOR, G. I. 1951 Analysis of the swimming of microscopic organisms. *Proc. R. Soc. Lond.* A **209**, 447–462.

TAYLOR, G. I. 1952 The action of waving cylindrical tails in propelling microscopic organisms. *Proc. R. Soc. Lond.* A **211**, 225–239.

TRAN-CONG, T. & PHAN-THIEN, N. 1986 Boundary element solution for half space elasticity or Stokes problems with no-slip boundary. *Comp. Mech.* **1**, 259–268.

YOUNGREN, G. K. & ACRIVOS, A. 1975 Stokes flow past a particle of arbitrary shape: a numerical method of solution. *J. Fluid Mech.* **69**, 377–403.